Investigation of soot morphology and particle size distribution in a turbulent nonpremixed flame via Monte Carlo simulations

Ahmed Abdelgadir*[a], Marco Lucchesi[b], Antonio Attili[a], Fabrizio Bisetti[a]

[a]Clean Combustion Research Center, King Abdullah University of Science and Technology, Saudi Arabia
[b]Dipartimento di Ingegneria Meccanica ed Aerospaziale, Università "La Sapienza" di Roma, 00184 Rome, Italy

Abstract

Recently, our group performed a set of direct numerical simulations (DNS) of soot formation and growth in a *n*-heptane three dimensional non-premixed jet flame [Attili et al., Proc. Comb. Inst, 35, 2015], [Attili et al., Comb. Flame, 161, 2014], [Bisetti et al.,Trans of the Royal Soc, 372, 2014]. The evolution of species relevant to soot formation and growth have been sampled along a large number of Lagrangian trajectories in the DNS. In this work, the DNS results are post-processed to compute the soot evolution along selected Lagrangian trajectories using a Monte Carlo method. An operator splitting approach is adopted to split the deterministic processes (nucleation, surface growth and oxidation) from coagulation, which is treated stochastically. The morphological properties of soot and the particle size distribution are investigated. For trajectories that experience an early strong nucleation event, the particle size distribution is found to be bimodal, as the soot particles have enough time to coagulate and grow while it is unimodal for trajectories characterized by only late nucleation events. As a results, the average size distribution at two different crosswise positions in the flame is unimodal.

1 Introduction

Regulations on soot emissions from light road vehicles are becoming tighter and will be applied to particle sizes and number density. Therefore, there is a need to develop a good understanding of the particles size distribution and the effect of soot/chemistry/turbulent interaction on this distribution.

In order to study the particle size distribution, one needs to solve the population balance equations (PBEs), which describe the conservation of the particulate entities. The sectional representation for simulating aerosol dynamics developed by Gelbard et al. [1] is the most employed method for solving the PBEs and is based on dividing the particle size domain into sections. Other than sectional methods, the method of moments is widely used, and the idea is to solve a number of low order moments derived from the population balance equations. These moments provide information such as number density, volume fraction and surface density, etc. However, the source terms for these moments are not closed, and therefore a closure model needs to be introduced. Numerous closure models have been developed, such as quadrature and direct quadrature method of moments [2, 3], and interpolative closure [4]. Whereas the method of moments is computationally tractable, the complexity of physical models for aerosol dynamics complicates the closure and information on the particle size distribution is not available.

*Corresponding author
Email addresses: ahmed.abdelgadir@kaust.edu.sa (Ahmed Abdelgadir) marco.lucchesi@uniroma1.it (Marco Lucchesi)
Proceedings of The European Combustion Meeting 2015

The most widely used technique for measuring the particle size distribution function (PSDF) experimentally is the scanning mobility particle sizer (SMPS) [5]. This technique relies on probe sampling from the flame and passing the sample to the scanning mobility particle sizer. The sampling technique is very sensitive to the perturbation induced by the probe as well as particle loss and growth due to coagulation in the probe and sampling tube, which must be carefully avoided to prevent inaccurate measurement of the PSDF. In addition to sampling difficulties, the instruments used to measure the PSDF also suffer from limitations in detection sizes and measurements are time-averaged over several minutes. Another technique that is widely used for measuring the soot quantities (e.g. soot volume fraction, number density and soot morphology) is Laser Induced Incandescence (LII) [6]. All measurement techniques such as Line of Sight Attenuation (LOSA) and LII, except the SMPS (which is not temporally resolved), only provide mean values of the soot morphological quantities, such as the mean primary particle diameter instead of the particle size distribution [7].

Most of the studies of the particle size distribution function (PSDF) in flames were performed on laminar flames configurations both experimentally and numerically reflecting the challenges in applying soot diagnostics in unsteady turbulent flames, and the enormous computational cost of performing DNS of turbulent sooting flames. A stochastic simulation approach has been proposed by Balthasar and Kraft [8] to study the particle size distribution in flames, with all aerosol processes treated in a stochastic manner. For each time step, only one aerosol process is solved depending on which process has been selected randomly. A majorant kernel was used in-

stead of the actual coagulation kernel, in order to speed up the calculations. Balthasar and Kraft [8] implemented this method to the calculation of soot in laminar premixed flames aiming to compare the results to the results obtained with a method of moments. A good agreement was found between the two methods for the first two moments.

Abid et al. [9] studied the PSDF for four different premixed ethylene-oxygen-argon flames via SMPS and aerosol electrometer [10]. The focus of their study was to investigate the bimodality of the PSDF. For all flames, a bimodal behavior of the PSDF was found. Zhao et al. [11] used the stochastic algorithm of [8] in laminar premixed ethylene flames. They found that the PSDF evolved from a power law function to bimodal distribution downstream. Singh et al. [12] implemented the same stochastic approach in laminar flames to study and compare the PSDF to experimental data [13]. A good agreement was found for the unimodal PSDF, while the cases with bimodal distribution were not computed accurately.

In this work, statistics of the size distribution of soot particles and aggregates across a turbulent nonpremixed flame are computed. The particle size distribution and the morphological properties are simulated for two different crosswise locations in the flame. The paper is organized as follows. First the physical models describing the aerosol dynamics are introduced. Second, the Monte Carlo algorithm for solving the dynamics processes is briefly introduced. Then, the flame studied is presented. Finally, the results obtained are discussed.

2 Physical models

In this study, a single soot aggregate is characterized by its volume V and surface S. A soot aggregate is composed by n_p primary particles, with average diameter d_p [14]. Soot aggregate volume and surface are expressed as:

$$V = \frac{\pi}{6} n_p d_p^3, \quad S = \pi n_p d_p^2. \tag{1}$$

The evolution of the soot population number density function (NDF) $n(V, S, t)$, is described by the Population Balance Equation.

$$\frac{\partial n}{\partial t} + \nabla \cdot n\mathbf{u} = \nabla \cdot D \nabla n + I_{nuc} + G_{cond} + S_{surf} + C_{coag}, \tag{2}$$

where $\mathbf{u}$ is the gas velocity and D is the diffusion coefficient. Soot particles have a high Schmidt number, therefore the diffusion is neglected. After neglecting the diffusion term, Eq. 2 may be recast in Lagrangian framework as

$$\frac{\partial \hat{n}}{\partial t} = I_{nuc} + G_{cond} + S_{surf} + C_{coag}, \tag{3}$$

where the terms on the right hand side represent the nucleation, condensation, surface reaction, and coagulation source term, respectively and $\hat{n}$ is the NDF along the Lagrangian trajectory.

The details of the soot models can be found in [15] and references therein. The nucleation of a soot particle is assumed to occur when two naphthalene dimers collide. Condensation is the collision between a naphthalene dimer and a soot particle. The surface reactions in this study include the surface growth by HACA (Hydrogen-Abstraction-C_2H_2-Addition) [16] and oxidation by oxygen and hydroxyl radical. Oxidation by OH is taken from Neoh et al. [17]. Oxidation reaction rates by O_2 are given in [18]. Coagulation is a collision of two soot particles.

3 Monte Carlo method

In Eq. 3, the source terms on the right hand side have different physical time scales. Operator splitting is an ideal approach to tackle such a problem. In this Monte Carlo scheme, the deterministic processes (nucleation, condensation, surface growth and oxidation) are treated seperatley from coagulation, which is treated stochastically. This scheme provides the flexibility of the stochastic simulation and the accuracy of the deterministic solution. A first order Lie splitting strategy (the least expensive scheme) is found to be adequate for this work.

Figure 1 shows a flowchart for all aerosol processes with the first order Lie scheme. In this scheme, the deterministic processes are solved first. To start the simulation, a certain number of notional particles and the reactor volume are specified, according to the initial soot number density. The nucleation term is addressed deterministically as a function of naphthalene concentration. In the last step of the deterministic simulation, condensation and surface reactions are treated by allowing the notional particles to interact with the background gaseous species.

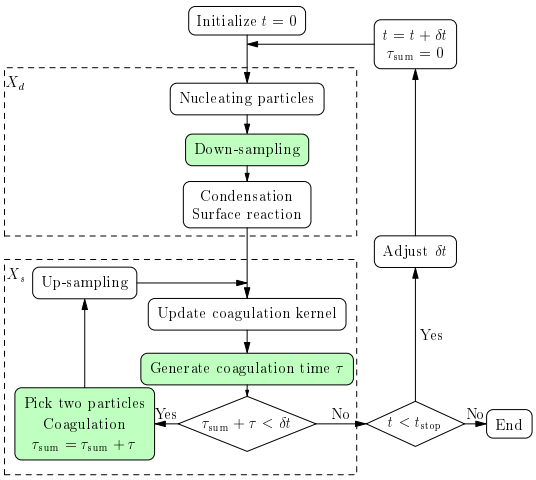

Figure 1: Monte Carlo flow chart.

Nucleation adds a number of notional particles into the stochastic reactor. Conversely, coagulation decreases the number of notional particle in the stochastic reactor. Since nucleation and coagulation may change the number of notional particles to values that are too large in terms of computational cost or too small in terms of the accu-

rate representation of the PSDF, upper and lower limits are prescribed. In case the number exceeds the allowed maximum N, the particles are down-sampled to N and the volume is adjusted accordingly to keep the number density consistent. When the number of particles decreases to the lower limit, the particles are doubled and so is the reactor volume. The accuracy of the Monte Carlo method depends on the maximum number of particles N. In the current work, 20,000 particles are used. In order to reduce stochastic noise, each simulation is repeated 120 times and the results are averaged.

The stochastic algorithm of Gillespie [19] is implemented for the simulation of soot particles coagulation. The coagulation kernel is the collision frequency of two soot particles in the free molecular regime.

$$\beta_{i,j} = 2.2 \left(\frac{\pi k T}{2\rho_{soot}}\right)^{0.5} \left(\frac{1}{V_i} + \frac{1}{V_j}\right)^{0.5} (dc_i + dc_j)^2, \tag{4}$$

where the factor 2.2 in Eq. 4 is the Van Der Waals enhancement factor [20], d_c is the collision diameter [21], and $D_f = 1.8$ is the fractal dimension of soot particles.

The simulation algorithm is as follows:

- Step 0: Specify initial values (volume, surface, diameter etc.) for N particles, determine the simulator size $V = \frac{N}{n_0}$,, where n_0 is the initial number density, and evaluate the pair coagulation rate matrix C:

$$C_{ij} = \frac{\beta_{i,j}}{V}, \quad i = 1, \ldots, N-1, j = i+1, \ldots, N.$$

- Step 1: Generate a random time τ at which two particles coagulate, by generating a random number r_1 from the uniform distribution in the unit interval

$$\tau = C_0^{-1} ln 1/r_1. \tag{5}$$

  Here C_0 is the summation of all pair coagulation rates, $C_0 = \sum_{i=1}^{N-1} \sum_{j=1}^{i+1} C_{ij}$.

- Step 2: Randomly choose two particles to coagulate according to the distribution $P(i,j) = C_{ij}/C_0$.

- Step 3: Update N (one particle less) and C_{ij}, and repeat Steps 1 and 2, until the accumulated random time τ is larger than the splitting time step δt used for the deterministic processes.

For a more detailed explanation of Monte Carlo approach and the partial conditioning method used for the treatment of step 2, the reader is referred to Gillespie [19].

4 Flame configuration

The formation, growth, and transport of soot have been investigated recently via large scale direct numerical simulation (DNS) in a three-dimensional temporally evolving planer jet non-premixed flame of nheptane and air with a jet Reynolds number of 15,000 [15, 22, 23]. A detailed chemical mechanism, which includes the soot precursor naphthalene, and a high-order method of moments were employed in the DNS. The evolution of the soot particles was described with moments derived from the population balance equation. The resulting moment transport equations are solved with a Lagrangian numerical scheme [24]. The source terms in the moment equations are closed using the hybrid method of moments (HMOM) [25].

The Lagrangian scheme used in the DNS allows to sample the species concentration and other quantities relevant to soot formation and growth along Lagrangian trajectories as a function of time. Figure 2 shows an example of the evolution of temperature, mixture fraction, and naphthalene mass fraction along one selected Lagrangian trajectory.

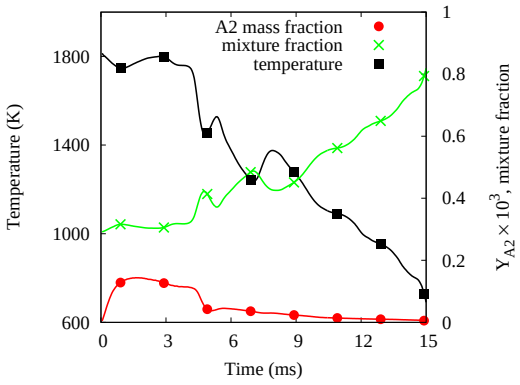

Figure 2: Evolution of selected scalar quantities as a function of time along a single Lagrangian trajectory.

5 Results

The DNS results are post-processed using a Monte Carlo method and the soot evolution along selected Lagrangian trajectories is simulated. The goals of this work is to study the soot/chemistry/turbulent interaction and the effect on the soot size distribution as well as the morphological properties of soot.

Two sets of Lagrangian trajectories are investigated:

- a first set A consists of 166 trajectories, which terminate on the flame centerline at time $t = 15\ ms$ of the DNS. At time $t = 15\ ms$ the planar temporal-evolving flame has reached a fully turbulent state.

- a second set B consists of 94 trajectories located at $15\ ms$ in a different crosswise position in the flame ($r/H \approx 0.75$). This correspond to the position of the maximum average soot mass fraction.

The selection of the first set is equivalent to the extraction of soot particles via probe techniques on the centerline of a turbulent flame at a given axial location. The second set corresponds to a different radial position in

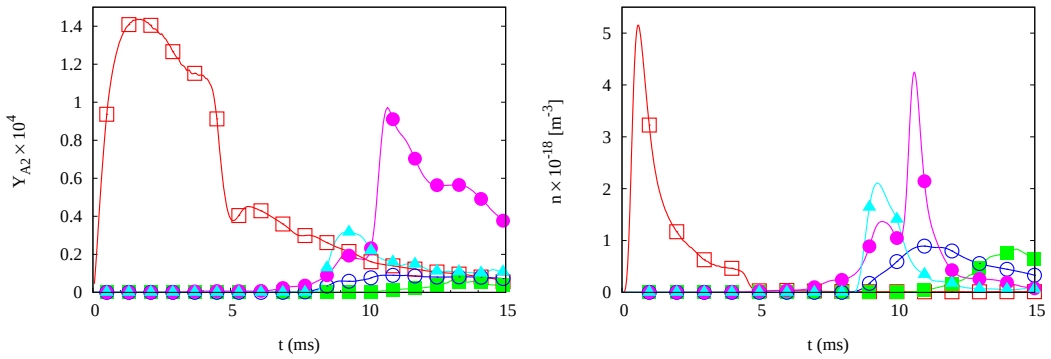

(a) naphthalene (A2) mass fraction.

(b) number density.

Figure 4: naphthalene (A2) and number density history for the 5 selected trajectories shown in Fig. 3.

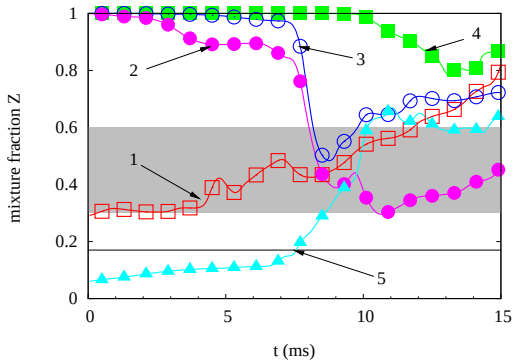

Figure 3: Evolution of mixture fraction along five trajectories selected randomly from set A. The gray region is the mixture fraction interval where high naphthalene concentration is observed. The horizontal black line marks the position of the flame in mixture fraction space.

the flame. Even if the selection of the Lagrangian trajectories is constrained, significant variations in the mixture fraction history among trajectories in the same set is observed. Trajectories start from different locations and drift through different regions. In Fig. 3, the mixture fraction history along five Lagrangian trajectories selected randomly is shown. All of them, except trajectory 5, start from different points in the rich flame region and follow various paths, moving to richer regions or drifting to leaner regions passing through different locations in mixture fraction space. This strong variability in mixture fraction space is reflected on the naphthalene concentration: trajectories reveal different histories in naphthalene concentration space, as it is shown in Fig. 4(a). It has been observed that a high naphthalene concentration occurs when mixture fraction lies in the interval $Z = 0.3$ and $Z = 0.6$ region [15, 26], which is marked in gray in Fig.3. Since naphthalene concentration determines nucleation and growth by condensation, this variability determines different soot histories, yielding different number density profiles in time, as well as different particle size distributions, both along single trajectories and at the final time for different trajectories. The PDFs are calculated for the collision diameter with fractal dimension $D_f = 1.8$. Figure 5(a) shows the PDF for the five selected trajectories at $t = 15$ ms. The results are compared with the average PDF. The average PDF for each of the two sets A and B is calculated by considering all the soot partilces in every trajectory in the set. The PDF for different trajectories show significant differences: while trajectories 1, 2 and 5 show a bimodal PDF, with a first peak at the size of nucleated particles and a second one at larger particle size, the PDFs for trajectories 3 and 4 have one peak, at nucleated particle size and a broad tail. The average PDF has only one peak at nucleated particle size and a broad tail. This strong difference in PDFs between single trajectories is related to the trajectory history. Turbulence is the main cause for such different histories, that are not observable in a laminar flame.

Number density is driven by nucleation, particles consumption due to the oxidation of very small particles, and by coagulation. Turbulence affects these processes by imposing a certain path on the Lagrangian trajectories and imposing a local scalar dissipation rate, influencing naphthalene concentration [15]. In Fig. 4(b) number density is shown as a function of time for the 5 selected trajectories. As evident from Fig. 5(a), particle size distributions appear to be both bimodal and unimodal; this difference can be explained by examining the number density history. Trajectories experiencing nucleation events (strong growth in the number density) at a late time have a uninomodal PDF. For trajectory 4 the only significant number density peak is at 14 ms, so coagulation and condensation have limited time to generate aggregates larger than nucleated particles, so the PDF tail is not very broad. For trajectory 3, the last number density peak is at 13 ms, and coagulation and condensation have twice the time to generate larger aggregates than for trajectory 4, hence, the tail is broader. Trajectory 2 experienced strong nucleation at 10 ms, so again coagulation and condensation result in larger aggregates that give rise to the second peak. Similar arguments apply to trajectory 1, that shows a second peak at even larger sizes, since it experiences a nu-

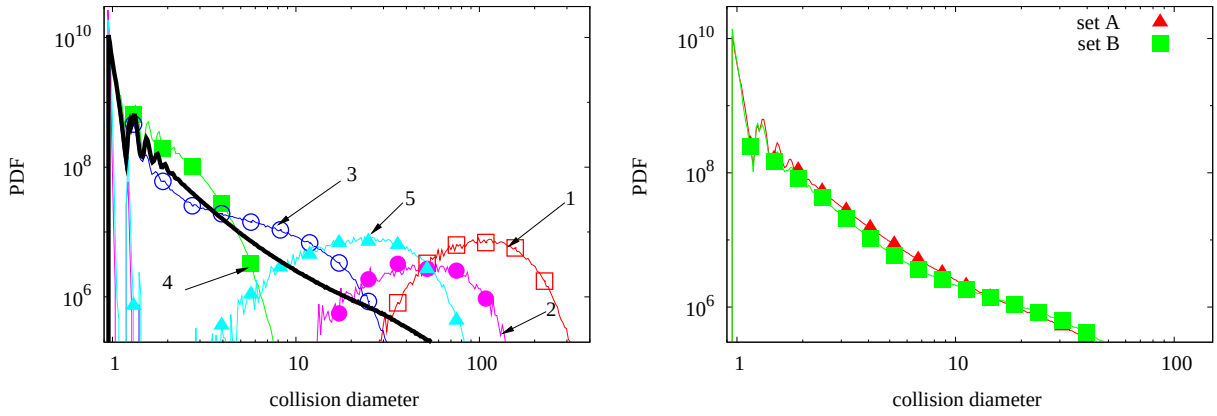

(a) particle size distribution at final time, black line is the average PDF.

(b) average PDF for the two sets.

Figure 5: PDFs for the 5 selected trajectories from set A and average PDF for sets A and B at 15 ms.

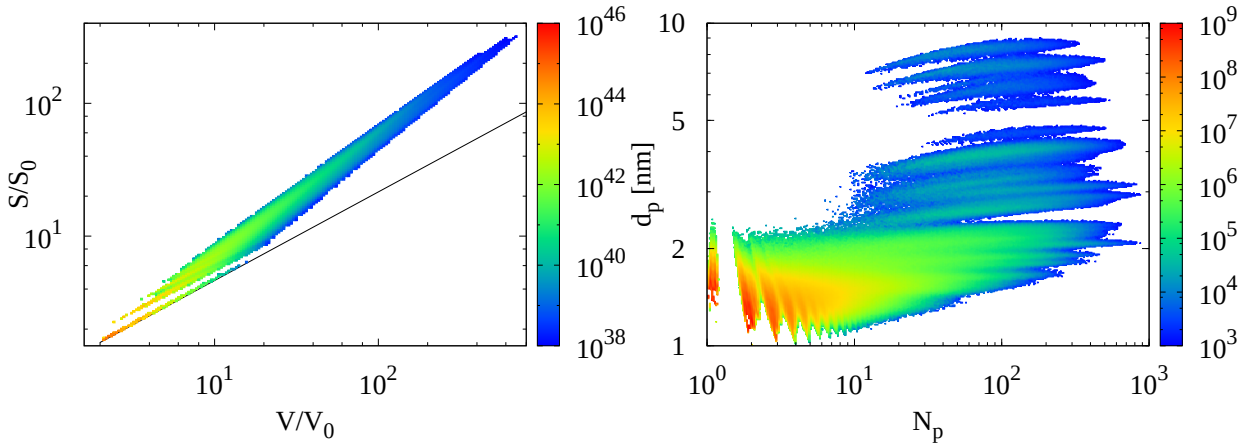

(a)

(b)

Figure 6: Bivariate particle size distribution in the sample space (V, S) at final time $t = 15\ ms$, normalized by volume and surface of nucleated particle (the line represent the spherical aggregate distribution), and bivariate particle size distribution in the primary particle descriptors set (N_p, d_p).

cleation event at a very early time.

The average PDF for the two sets A and B are compared in Fig. 5(b). The two sets are almost identical and show a uninomodal PDF with a broad tail, extending over two orders of magnitude in diameter. The PDFs show that the soot population is composed mainly of small particles and aggregates. The bivariate PDF in the space of volume and surface normalized by nucleated particle volume and surface is shown in Fig. 6(a). Only the bivariate PDF for set A are presented. In Fig. 6(a), a line has been plotted, representing spheres. The distributions are bow-shaped laying above the spherical aggregate line, peaking at the nucleated particle size. The distribution is steeper than the spherical aggregate distribution, so for every possible volume the surface area is larger than the corresponding spherical area, highlighting the aggregate-like morphology of soot. The larger the volume, the more the surface is larger than a sphere of corresponding volume. Primary particles number per aggregate and diameter are obtained as fractional moments of the particle size distribution. The bivariate distribution of these two variables provides an insight on soot aggregate morphology, and it is reported in Fig. 6(b). The distribution peaks at small diameter and number per aggregate values, confirming that soot population is composed by very small particles. It is also apparent that aggregates with large number of primary particles are made of large primary particles and vice versa.

6 Conclusions

The evolution of the particle size distribution and morphology are simulated in turbulent nonpremixed flame using a Monte Carlo approach. An operator splitting technique is adopted in these simulations to separate deterministic processes from the stochastic processes, thereby making those calculation tractable for a large number of cases and repetitions. The simulations are per-

formed along selected Lagrangian trajectories extracted from a DNS of nonpremixed n-heptane planer jet flame where all species relative to soot formation and growth are sampled. The shape of the PDF at the end of the trajectory is determined by the trajectory history which is controlled by turbulence fluctuations. For trajectories that experience a single and early strong nucleation event, the PDF is found to be bimodal, as the soot particles have enough time to coagulate and grow. The PDFs of the soot particles on Lagrangian trajectories show that the population is mainly composed by small particles. The bivariate PDF in volume and surface shows that large aggregates are most likely for soot cluster of larger volume and the bivariate PDF in primary particle descriptors shows that the aggregate with a large number of primary particle are made of large primary particles and vice versa.

References

[1] F. Gelbard, Y. Tambour, J. H. Seinfeld, Journal of Colloid and Interface Science 76 (1980) 541–556.

[2] R. McGraw, Aerosol Science and Technology 27 (1997) 255–265.

[3] D. L. Marchisio, R. O. Fox, Journal of Aerosol Science 36 (2005) 43–73.

[4] M. Frenklach, Chemical Engineering Science 57 (2002) 2229–2239.

[5] B. Zhao, Z. Yang, J. Wang, M. V. Johnston, H. Wang, Aerosol Science & Technology 37 (2003) 611–620.

[6] R. J. Santoro, C. R. Shaddix, Applied combustion diagnostics (2002) 252–286.

[7] A. E. Karataş, Ö. L. Gülder, Progress in Energy and Combustion Science 38 (2012) 818–845.

[8] M. Balthasar, M. Kraft, Combustion and Flame 133 (2003) 289–298.

[9] A. D. Abid, N. Heinz, E. D. Tolmachoff, D. J. Phares, C. S. Campbell, H. Wang, Combustion and Flame 154 (2008) 775–788.

[10] A. Abid, E. Tolmachoff, D. Phares, H. Wang, Y. Liu, A. Laskin, Proceedings of the Combustion Institute 32 (2009) 681–688.

[11] B. Zhao, Z. Yang, M. V. Johnston, H. Wang, A. S. Wexler, M. Balthasar, M. Kraft, Combustion and Flame 133 (2003) 173–188.

[12] J. Singh, R. I. Patterson, M. Kraft, H. Wang, Combustion and Flame 145 (2006) 117–127.

[13] B. Zhao, Z. Yang, Z. Li, M. V. Johnston, H. Wang, Proceedings of the Combustion Institute 30 (2005) 1441–1448.

[14] S. Park, S. Rogak, Aerosol Science & Technology 37 (2003) 947–960.

[15] A. Attili, F. Bisetti, M. E. Mueller, H. Pitsch, Combustion and Flame (2014).

[16] M. Frenklach, H. Wang, in: Symposium (International) on Combustion, volume 23, Elsevier, pp. 1559–1566.

[17] K. Neoh, J. Howard, A. Sarofim, in: D. Siegla, G. Smith (Eds.), Particulate Carbon, Springer US, 1981, pp. 261–282.

[18] A. Kazakov, H. Wang, M. Frenklach, Combustion and Flame 100 (1995) 111–120.

[19] D. T. Gillespie, Journal of the Atmospheric Sciences 32 (1975) 1977–1989.

[20] S. J. Harris, I. M. Kennedy, Combustion science and technology 59 (1988) 443–454.

[21] F. E. Kruis, K. A. Kusters, S. E. Pratsinis, B. Scarlett, Aerosol science and technology 19 (1993) 514–526.

[22] F. Bisetti, A. Attili, H. Pitsch, Phil. Trans. of the Royal Soc. A, submitted (2014).

[23] A. Attili, F. Bisetti, M. E. Mueller, H. Pitsch, Proceedings of the Combustion Institute (2014).

[24] A. Attili, F. Bisetti, Computers & Fluids 84 (2013) 164–175.

[25] M. Mueller, G. Blanquart, H. Pitsch, Combustion and Flame 156 (2009) 1143–1155.

[26] F. Bisetti, G. Blanquart, M. E. Mueller, H. Pitsch, Combustion and Flame 159 (2012) 317–335.